VNU Journal of Science: Mathematics – Physics, Vol. 38, No. 1 (2022) 65-75

VNU Journal of Science: Mathematics - Physics

Journal homepage: https://js.vnu.edu.vn/MaP

Original Article

Structural and Electrical Properties of Samarium-doped Ceria Electrolyte

Dang Thanh Hai[1], Vu Van Hung[2], Pham Ngoc Thu[3], Lo Ngoc Dung[3], Le Thi Thanh Huong[4], Hoang Thi Minh Anh[5], Le Thu Lam[3,*]

[1]*Vietnam Education Publishing House, 81 Tran Hung Dao, Hoan Kiem, Hanoi, Vietnam*
[2]*VNU University of Education, 182 Luong The Vinh, Thanh Xuan, Hanoi, Vietnam*
[3]*Tay Bac University, Chu Van An, Quyet Tam, Sonla, Vietnam*
[4]*Hai Phong University, 171 Phan Dang Luu, Kien An, Haiphong, Vietnam*
[5]*Quang Trung Primary School, 27 Tran Quang Dieu, Quang Trung, Thaibinh, Vietnam*

Received 6 July 2021
Revised 26 August 2021; Accepted 29 August 2021

Abstract: Effect of dopant on structural and electrical properties of samarium-doped ceria (SDC) electrolyte was investigated using statistical moment method. Our results showed the lattice expansion due to doping and local distortion resulting from preferential distribution of oxygen vacancies around dopants. The ionic conductivity of SDC crystals is in more than three orders of magnitude larger than that of pure ceria. However, the presence of dopant in cation edge and the first nearest neighbor positions around migrating vacancy gives rise to the blocking and trapping effects on the vacancy transport. The maximum value of the ionic conductivity was found for the samples with the dopant concentration x = 0.15. These results can be compared to the one of the published data of boththe theoretical and experimental investigations

Keywords: Samarium-doped ceria, structural property, electrical property, ionic conductivity.

1. Introduction

Solid oxide fuel cells (SOFCs) is an electrochemical conversion device that produces electricity directly from the oxidation of hydrogen or hydrogen-rich fuels in environmentally benign way [1, 2]. SOFCs provide the clean energy with high efficiency, notably fuel flexibility and therefore become one of the most promising technologies for future applications related to energy conversion and

* Corresponding author.
E-mail address: lethulam@utb.edu.vn

https//doi.org/10.25073/2588-1124/vnumap.4660

storage. For efficient performance, SOFCs require electrolytes with a large oxygen ion conductivity. For the traditional SOFCs with 8 mol% yttria-stabilized zirconia (YSZ) as a standard electrolyte material, to fulfill the requirement of oxygen ion conduction, the operation temperature can be as large as around 1000^{o}C [3]. However, the high operating temperature will lead to thermal degradation, thermal expansion mismatch, and reaction between the cell components and thus lower useful lifetime of SOFCs [4]. So far, ceria doped with rare earth elements like Sm, Nd, Gd, etc. as alternative solid electrolytes for YSZ has a large ionic conductivity at the low and intermediate temperatures [5]. Among the ceria-based electrolytes, samarium-doped ceria (SDC) was reported to have the largest conductivity at the same dopant concentration [6].

Experimentally, the structural and electrical properties of SDC crystals were determined at a wide range of temperatures and the various dopant concentrations using X-ray diffraction combined with conventional d.c. four-probe measurements [7], open circuit voltage [8], direct current polarization [10], and impedance spectroscopy [9, 11] measurements with strikingly different results. The lattice constant increased sharply with the dopant concentration x [8,11] and the solubility limit of samarium in a fluorite lattice was found as $0.4 < x < 0.6$ [7]. The dependences of the ionic conductivity on the temperature, dopant content [7, 8, 11], oxygen partial pressure [10], elastic lattice strain [9], and the role of the grain boundary conductivity were evaluated in detail [11, 12]. The ionic conductivity was measured as a nonlinear function of the dopant concentration and the maximum value obtained at x = 0.2 [7], x = 0.15 [8], x = 0.1 [9, 12], x = 0.07 [11] in the temperature range of 400 ^{o}C-900 ^{o}C. These results were scattered widely because they were highly dependent on the synthesis preparation of samples and measurement techniques. On the computational side, the electrical property of SDC crystals was investigated basing on two contributions on ionic conductivity: i) The vacancy migration energy across the common edge of two adjacent tetrahedra containing cations; and ii) The association energy between oxygen vacancy and dopant [13-15]. Combining Metropolis and Kinetic Monte Carlo (KMC) simulations, Grieshammer et al., [13] suggested an increase in the migration energy with the increasing number of Sm^{3+} ions in the common cation edge of two adjacent tetrahedra. Using the density functional theory (DFT), Fu et al., [14] showed that the samarium concentration could play an important role in the activity of vacancy migration and the association between oxygen vacancy and dopant. Nevertheless, employing simulations and DFT method require heavy computational workloads. Using extrapolation method, the calculated lattice parameter had some errors due to linearly fitting the apparent lattice parameter and $\cos^2\theta$ [16]. Furthermore, the trapping effect for the vacancy migration has not been fully evaluated to understand the existence of maximum value in ionic conductivity of SDC crystals.

Lately, the statistical moment method (SMM) has been developed to gain insight into the diffusion and electrical properties of yttria-doped ceria (YDC) and yttria-stabilized zirconia (YSZ with fluorite structure [17, 18]. The explicitly analytic expressions of the vacancy migration and dopant-vacancy association energies were derived from the Helmholtz free energy. In this study, we consider the structural property of SDC crystals related to the lattice strain resulting from Sm-doping and the association between oxygen vacancy and dopant. The role of dopant on the electrical property of SDC crystals is highlighted through the blocking and trapping effects for the vacancy hopping. The dopant concentration dependence of the ionic conductivity is evaluated in detail. This study provides more insight into the atomistic level picture of the influence of dopant on the structural and electrical properties of SDC crystals.

2. Theory

Pure ceria CeO_2 itself is not a good ionic conductor. Doping of CeO_2 with Sm_2O_3 generates the

numerous oxygen vacancy to satisfy the charge neutrality of the crystalline lattice. The oxygen vacancy formation in SDC crystals is described in Kröger-Vink notation as follows [13]

$$Sm_2O_3 \rightarrow 2Sm_{Ce}^{'} + 3O_O^x + V_O^{\bullet\bullet}, \tag{1}$$

Consequently, the oxygen vacancies $V_O^{\bullet\bullet}$ are the majority charged carriers with the content controlled by the dopant content, $\left[V_O^{\bullet\bullet}\right] = \frac{1}{2}\left[Sm_{Ce}^{'}\right]$. The chemical formula of SDC crystals taking into account the ionic concentration can be written as $Ce_{1-x}Sm_xO_{2-x/2}$, with x is the concentration of Sm^{3+} ions. Consequently, the number of Sm^{3+} ions is denoted as N then the numbers of Ce^{4+} and O^{2-} ions are $N(1-x)$ and $N(2-x/2)$, respectively.

2.1. Anharmonic Oscillation and Helmholtz Free Energy

In the SMM, $Ce_{1-x}Sm_xO_{2-x/2}$ crystal is described by the anharmonic vibrations of Ce^{4+}, Sm^{3+}, and O^{2-} ions with the Hook constants k_{Ce}, k_{Sm}, k_O, the oscillation frequencies ω_{Ce}, ω_{Sm}, ω_O, and the nonlinear parameters β_O, γ_1^{Ce}, γ_1^{Sm}, γ_1^O, γ_2^{Ce}, γ_2^{Sm}, γ_2^O, γ_{Ce}, γ_{Sm}, γ_O, [19]

$$k_{Ce,Sm,O} = \frac{1}{2}\sum_i \left(\frac{\partial^2 \varphi_{i0}^{Ce,Sm,O}}{\partial u_{i\beta}^2}\right)_{eq} = m^* \omega_{Ce,Sm,O}^2, \quad x_{Ce,Sm,O} = \frac{\hbar\omega_{Ce,Sm,O}}{2\theta}, \tag{2}$$

$$\beta = \frac{1}{2}\sum_i \left(\frac{\partial^3 \varphi_{i0}^{O}}{\partial u_{i\alpha}\partial u_{i\beta}\partial u_{i\gamma}}\right)_{eq}, \quad K = k_O - \frac{\beta^2}{3\gamma_O}, \tag{3}$$

$$\gamma_1^{Ce,Sm,O} = \frac{1}{48}\sum_i \left(\frac{\partial^4 \varphi_{i0}^{Ce,Sm,O}}{\partial u_{i\beta}^4}\right)_{eq}, \quad \gamma_2^{Ce,Sm,O} = \frac{1}{8}\sum_i \left(\frac{\partial^4 \varphi_{i0}^{Ce,Sm,O}}{\partial u_{i\alpha}^2 \partial u_{i\beta}^2}\right)_{eq}, \tag{4}$$

$$\gamma_{Ce,Sm,O} = 4\left(\gamma_1^{Ce,Sm,O} + \gamma_2^{Ce,Sm,O}\right), \tag{5}$$

where $\beta = x, y,$ or z, $u_{i\beta}$ denotes β-Cartesian component of the ionic displacement of ith ion, φ_{io}^{Ce} (or φ_{io}^{Sm} or φ_{io}^{O}) is the interaction potential between 0th and ith Ce^{4+} (or Sm^{3+}, or O^{2-}) ions, and m is the average atomic mass.

The thermal expansion of $Ce_{1-x}Sm_xO_{2-x/2}$ crystal is determined through the average nearest-neighbor distance (NND) $r_1(T)$ between two intermediate ions at the temperature T

$$r_1(T) = r_1(0) + C_{Ce}y_0^{Ce}(T) + C_{Sm}y_0^{Sm}(T) + C_O y_0^O(T), \tag{6}$$

with $r_1(0)$ is the average NND at $T = 0$ K, C_{Ce}, C_{Sm}, C_O are the concentrations of Ce^{4+}, Sm^{3+}, and O^{2-} ions, respectively, and y_0^{Ce}, y_0^{Sm}, y_0^O are the displacements of Ce^{4+}, Sm^{3+}, and O^{2-} ions, respectively, from the equilibrium position. Using the SMM, one can determine these displacements taking into account the anharmonic effects of the lattice vibrations by

$$y_0^{Ce}(T) \approx \sqrt{\frac{2\gamma_{Ce}\theta^2}{3k_{Ce}^3}A_{Ce}}, \qquad y_0^{Sm}(T) \approx \sqrt{\frac{2\gamma_{Sm}\theta^2}{3k_{Sm}^3}A_{Sm}}, \tag{7}$$

$$y_0^O(T) \approx \sqrt{\frac{2\gamma_O\theta^2}{3k_O^3}A_O} - \frac{\beta}{3\gamma_O} + \frac{1}{K}\left(1+\frac{6\gamma_O^2\theta^2}{K^4}\right)\left[\frac{1}{3}+\frac{\gamma_O\theta}{3k_O^2}(X_O-1)-\frac{2\beta^2}{27\gamma_O k_O}\right], \quad (8)$$

with the parameters A_{Ce}, A_{Sm} and A_O are determined as Ref. [21].

Because $Ce_{1-x}Sm_xO_{2-x/2}$ crystal is built by substituting N_{Sm} ions Sm^{3+} into the positions of Ce^{4+} ions of $CeO_{2-x/2}$ crystal, the Helmholtz free energy of $Ce_{1-x}Sm_xO_{2-x/2}$ crystal has an approximate form as

$$\Psi \approx \Psi_{CeO_{2-x/2}} + \Psi_{Sm} - N_{Sm}u_0^{Ce} - TS_c^*, \quad (9)$$

with $\Psi_{CeO_{2-x/2}}$ is the total Helmholtz free energy of $CeO_{2-x/2}$ crystal that is determined through the Helmholtz free energies of Ce^{4+} and O^{2-} ions [19-21], Ψ_{Sm} is the Helmholtz free energy of Sm^{3+} ions in $Ce_{1-x}Sm_xO_{2-x/2}$ crystal, and S_c^* is the configuration entropy. Based on the moment expansion analysis in quantum statistical physics [19,21], the Helmholtz free energies of Ce^{4+} and O^{2-} ions in $CeO_{2-x/2}$ crystal, and the Helmholtz free energy of Sm^{3+} ions in $Ce_{1-x}Sm_xO_{2-x/2}$ crystal are given by

$$\Psi_{Ce} = U_0^{Ce} + 3N_{Ce}\theta\left[x_{Ce} + \ln\left(1-e^{-2x_{Ce}}\right)\right] + 3N_{Ce}\left\{\frac{\theta^2}{k_{Ce}^2}\left[\gamma_2^{Ce}X_{Ce}^2 - \frac{2\gamma_1^{Ce}}{3}a_1^{Ce}\right] + \right.$$
$$\left. + \frac{2\theta^3 a_1^{Ce}}{k_{Ce}^4}\left[\frac{4}{3}\left(\gamma_2^{Ce}\right)^2 X_{Ce} - 2\left(\left(\gamma_1^{Ce}\right)^2 + 2\gamma_1^{Ce}\gamma_2^{Ce}\right)\left(1+X_{Ce}\right)\right]\right\}, \quad (10)$$

$$\Psi_{Sm} = U_0^{Sm} + 3N_{Sm}\theta\left[x_{Sm} + \ln\left(1-e^{-2x_{Sm}}\right)\right] + 3N_{Sm}\left\{\frac{\theta^2}{k_{Sm}^2}\left[\gamma_2^{Sm}X_{Sm}^2 - \frac{2\gamma_1^{Sm}}{3}a_1^{Sm}\right] + \right.$$
$$\left. + \frac{2\theta^3 a_1^{Sm}}{k_{Sm}^4}\left[\frac{4}{3}\left(\gamma_2^{Sm}\right)^2 X_{Sm} - 2\left(\left(\gamma_1^{Sm}\right)^2 + 2\gamma_1^{Sm}\gamma_2^{Sm}\right)\left(1+X_{Sm}\right)\right]\right\}, \quad (11)$$

$$\Psi_O = U_0^O + 3N_O\theta\left[x_O + \ln\left(1-e^{-2x_O}\right)\right] + 3N_O\left\{\frac{\theta^2}{k_O^2}\left[\gamma_2^O X_O^2 - \frac{2\gamma_1^O}{3}a_1^O\right] + \right.$$
$$\left. + \frac{2\theta^3 a_1^O}{k_O^4}\left[\frac{4}{3}\left(\gamma_2^O\right)^2 X_O - 2\left(\left(\gamma_1^O\right)^2 + 2\gamma_1^O\gamma_2^O\right)\left(1+X_O\right)\right]\right\} +$$
$$+3N_O\left\{\frac{\theta\beta}{6K\gamma_O}\left(\frac{k_O}{K}-1\right) + \frac{\theta^2\beta}{K}\left[\left(\frac{2\gamma_O a_1^O}{3K^3}\right)^{\frac{1}{2}} - \frac{\beta a_1^O}{9K^2} + \frac{\beta k_O a_1^O}{9K^3} + \frac{\beta}{6Kk_O}\left(X_O-1\right)\right]\right\}, \quad (12)$$

$$a_1^{Ce,Sm,O} = 1 + \frac{1}{2}X_{Ce,Sm,O}\coth X_{Ce,Sm,O},\ X_{Ce,Sm,O} = \frac{\hbar\omega_{Ce,Sm,O}}{2\theta},\ \theta = k_B T, \quad (13)$$

here, k_B is Boltzmann constant, U_0^{Ce}, U_0^{Sm}, U_0^O are the total interaction potentials of Ce^{4+}, Sm^{3+}, and O^{2-} ions at the equilibrium position, respectively. The total interaction potentials of Ce^{4+} and O^{2-} ions in $CeO_{2-x/2}$ crystal including the presence of oxygen vacancies can be determined as [18]

$$U_0^{Ce} = \frac{N_{Ce}}{2}\sum_i b_i^{Ce-Ce}\varphi_{i0}^{*Ce-Ce} + \frac{N_{Ce}N_O}{4N}\sum_i b_i^{Ce-O}\varphi_{i0}^{*Ce-O}, \quad (14)$$

$$U_0^O = \frac{N_O}{2}\sum_i b_i^{O-Ce}\varphi_{i0}^{*O-Ce} + \frac{N_O\left(N_O-1\right)}{2\left(2N-1\right)}\sum_i b_i^{O-O}\varphi_{i0}^{*O-O}, \quad (15)$$

The total interaction potential of Sm^{3+} ions is strongly impacted by the distribution of oxygen vacancies around Sm^{3+} ions in $Ce_{1-x}Sm_xO_{2-x/2}$ crystal. Due to the association between oxygen vacancy and dopant [13,14], the oxygen vacancies are preferentially located at the first nearest neighbor (1NN) or the second nearest neighbor (2NN) sites relative to Sm^{3+} ions. Based on probability theory, we find the expressions of total interaction potentials of Sm^{3+} ions in $Ce_{1-x}Sm_xO_{2-x/2}$ crystal in these two situation as:

$$U_{01NN}^{Sm} = \frac{N_{Sm}N_{Ce}}{2\left(N-1\right)}\sum_i b_i^{Sm-Ce}\varphi_{i0}^{*Sm-Ce} + \frac{N_{Sm}\left(N_{Sm}-1\right)}{2\left(N-1\right)}\sum_i b_i^{Sm-Sm}\varphi_{i0}^{*Sm-Sm} + \\ + \frac{N_{Sm}}{2}\sum_i b_i^{Sm-O}\varphi_{i0}^{*Sm-O} - \frac{N_{va}\left(N_{Sm}-1\right)}{2\left(N-4\right)}\sum_{i\geq 2} b_i^{Sm-O}\varphi_{i0}^{*Sm-O}, \quad (16)$$

$$U_{02NN}^{Sm} = \frac{N_{Sm}N_{Ce}}{2\left(N-1\right)}\sum_i b_i^{Sm-Ce}\varphi_{i0}^{*Sm-Ce} + \frac{N_{Sm}\left(N_{Sm}-1\right)}{2\left(N-1\right)}\sum_i b_i^{Sm-Sm}\varphi_{i0}^{*Sm-Sm} + \\ + \frac{N_{Sm}}{2}\sum_i b_i^{Sm-O}\varphi_{i0}^{*Sm-O} - \frac{N_{va}}{2}\varphi_{20}^{*Sm-O} - \frac{N_{va}\left(N_{Sm}-1\right)}{4\left(N-16\right)}\sum_{i\geq 3} b_i^{Sm-O}\varphi_{i0}^{*Sm-O}, \quad (17)$$

here, b_i^{X-Ce} (or b_i^{X-Sm}, or b_i^{X-O}) in Eqs. (14) - (17) is the number of the *i*th nearest-neighbor sites relative to X ion (X = Ce^{4+}, Sm^{3+}, O^{2-}) that Ce^{4+} (or Sm^{3+}, or O^{2-}) ions could occupy, respectively, φ_{i0}^{*X-Ce} (or φ_{i0}^{*X-Sm}, or φ_{i0}^{*X-O}) is the interaction potential between the 0th X ion and a Ce^{4+} (or Sm^{3+}, or O^{2-}) ion at the *i*th nearest-neighbor sites relative to this X ion, respectively.

2.2. Ionic Conductivity

The ionic conduction of $Ce_{1-x}Sm_xO_{2-x/2}$ crystal with fluorite structure is explained due to the oxygen vacancy-oxygen ion exchange occurred at the vacant sites on anion sub-lattice. The ionic conductivity can be straightforwardly computed by [18]:

$$\sigma = \frac{\sigma_0}{T}\exp\left(\frac{-E_a}{k_BT}\right), \quad (18)$$

where the pre-exponential factor σ_0 is given by

$$\sigma_0 = nq^2r_1^2n_1 f\,\frac{\omega_0}{2\pi}\exp\left(\frac{S_v^f}{k_B}\right), \quad (19)$$

where r_1 is the nearest distance between two lattice sites containing O^{2-} ions, n_1 is the number of O^{2-} ions at the 1NN positions to the oxygen vacancy, f the correlation factor, ω_O is oscillation frequency of O^{2-} ions around their equilibrium position, S_v^f is the entropy for the formation of an oxygen vacancy [22] and E_a is the activation energy for vacancy migration in the crystaline lattice. Due to doping, the activation energy is the sum of the oxygen vacancy-dopant association energy E_{ass} and the vacancy migration energy E_m [15]

$$E_a = E_{ass} + E_m . \quad (20)$$

The oxygen vacancy-dopant association energy can be considered as the energy change of the crystal containing the oxygen vacancies and Y^{3+} ions at the associated state and that containing the oxygen vacancies and Y^{3+} ions at the isolated state. In the previous studies [17, 18], we constructed the structural systems describing the different states of oxygen vacancies and Sm^{3+} ions in the crystal layer with the chemical formulas as $Ce_{N_{Ce}}Sm_{N_{Sm}}O_{N_O}$, $Ce_{N_{Ce}-1}Sm_{N_{Sm}+1}O_{N_O}$, $Ce_{N_{Ce}-2}Sm_{N_{Sm}+2}O_{N_O-1}$ and $Ce_{N_{Ce}-1}Sm_{N_{Sm}+1}O_{N_O-1}$. Then the vacancy-dopant association energy of $Ce_{1-x}Sm_xO_{2-x/2}$ crystal is given by

$$E_{ass} = \left(\Psi_{Ce_{N_{Ce}}Sm_{N_{Sm}}O_{N_O}} + \Psi_{Ce_{N_{Ce}-2}Sm_{N_{Sm}+2}O_{N_O-1}}\right) - \left(\Psi_{Ce_{N_{Ce}-1}Sm_{N_{Sm}+1}O_{N_O}} + \Psi_{Ce_{N_{Ce}-1}Sm_{N_{Sm}+1}O_{N_O-1}}\right), \quad (21)$$

where the Helmholtz free energies of these systems are calculated based on Eqs. (9) - (12).

The saddle point B is the midpoint between the initial A and final B positions after vacancy migration (Figure 1).

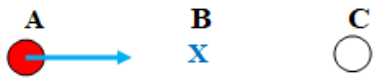

Figure 1. The hopping of an O^{2-} ion from lattice site A, across saddle point B and occupies an adjacent vacant site C. The oxygen ions and oxygen vacancies are red and white circles, respectively.

The vacancy migration corresponds to the movement of an O^{2-} ion in the opposite direction. Then the vacancy migration energy between adjacent oxygen lattice sites is determined as the free energy difference of the crystalline lattice at two states: after the oxygen moving to the saddle point (called saddle point state) and before the oxygen transporting from the lattice site (called as initial state) [17, 18].

$$E_m = \Psi_{saddle} - \Psi_0, \quad (22)$$

where Ψ_0 and Ψ_{saddle} are the initial and saddle point free energies, respectively. The total interaction potentials of Ce^{4+}, Sm^{3+}, and O^{2-} ions determining the saddle point energy are given by

$$U^{Ce}_{saddle} = U^{Ce}_0 + \frac{\varphi^B_{O-Ce} - \varphi^A_{O-Ce}}{2}, \quad (23)$$

$$U^{Sm}_{saddle} = U^{Sm}_0 + \frac{\varphi^B_{O-Sm} - \varphi^A_{O-Sm}}{2}, \quad (24)$$

$$U^{O}_{saddle} = U^{O}_0 + \frac{\varphi^B_{O-Ce} - \varphi^A_{O-Ce} + \varphi^B_{O-Sm} - \varphi^A_{O-Sm}}{2} + \frac{U^*_{O-O} - \Delta u^1_{O-O} + \Delta u^2_{O-O}}{2}, \quad (25)$$

where $\varphi^{A,B}_{O-Ce}$ (or $\varphi^{A,B}_{O-Sm}$) are the interaction potentials between the diffusing oxygen ion at sites A, B and surrounding Ce^{4+} (or Sm^{3+}) ions; U^*_{O-O} is the total interaction potential of (N_O +1) O^{2-} ions for interactions between them and surrounding oxygen ions if the vacant site C is occupied by an O^{2-} ion from outside; Δu^1_{O-O} is the total reciprocal interaction potential between O^{2-} ions at the sites A and C and surrounding O^{2-} ions; and Δu^2_{O-O} is the reciprocal interaction potential between the O^{2-} ion at the

site B and surrounding O^{2-} ions. Notably, Eqs. (23) - (25) are sensitive to the configurations of the nearest neighboring cations around A and B sites. As a result, the migration energies according to these different configurations can be derived.

3. Results and Discussion

The interaction between ions in $Ce_{1-x}Sm_xO_{2-x/2}$ crystal is described by pure Coulomb potential and Buckingham potential including the short-range interactions [23]

$$\varphi_{ij}(r) = \frac{q_i q_j}{r} + A_{ij}\exp\left(-\frac{r}{B_{ij}}\right) - \frac{C_{ij}}{r^6}, \quad (26)$$

where q_i, q_j are the charges of the *i*-th and *j*-th ions, r is the equilibrium distance between them, and A_{ij}, B_{ij}, C_{ij} are adjustable parameters extracted from simulation calculations (listed in Table 1).

Table 1. The parameters of the Buckingham potential in $Ce_{1-x}Sm_xO_{2-x/2}$ crystal [23].

Interaction	A_{ij} / eV	B_{ij} / Å	C_{ij} / $eV.Å^6$
O^{2-} - O^{2-}	9547.96	0.2192	32.00
Ce^{4+} - O^{2-}	1809.68	0.3547	20.40
Sm^{3+} - O^{2-}	1944.44	0.3414	21.49

The lattice parameter of SDC crystals can be derived from Eq. (6) based on the relation between the size $a(T)$ of unit cell and the NND $r_1(T)$ being $a(T) = 4/\sqrt{3}r_1(T)$. In Fig. 2, the lattice parameter of SDC crystals at the room temperature is plotted as a function of dopant concentration. The calculated lattice parameter is little larger than that of CeO_2 crystal (x = 0) and increases linearly with an increase in the dopant concentration until its solubility limit (x = 0.4).

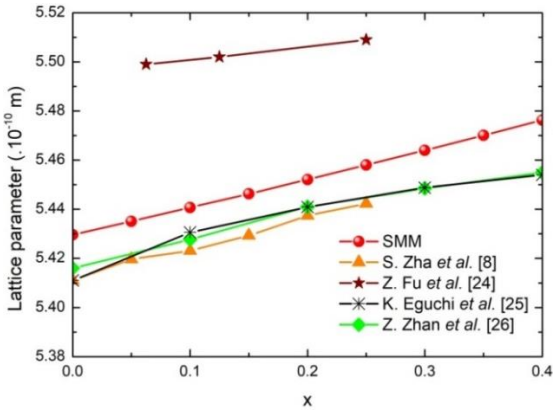

Figure 2. The lattice parameter at various dopant concentrations. The theoretical [24] and experimental [8, 25, 26] results are presented for comparison.

The lattice expansion due to Sm-doping is attributed to the larger radius of Sm^{3+} ions (1.09 Å) than that of Ce^{4+} ions (0.97 Å). As it can be seen from Fig. 2, our theoretical calculations are in good

accordance with the experimental results [8, 25, 26]. The lattice parameters obtained by X-ray diffraction [25, 26] increase rapidly with the increasing dopant concentration at $x \leq 0.2$ but change more slowly as the dopant concentration approaches its solubility limit, $x = 0.4$. Experimentally, the dissolution of Sm_2O_3 in the fluorite lattice is limited and consequently, the replacement of Ce^{4+} ions by Sm^{3+} ions occurs more difficult at the high dopant concentration. The first-principles results by Fu et al. [24] have larger values than the SMM results due to their models without oxygen vacancies.

Table 2 presents the vacancy-dopant association energies at the 1NN and 2NN positions around Sm^{3+} ion. The negative signs of the association energies indicate that the oxygen vacancies can be trapped at the 1NN and 2NN sites. However, the absolute value of E_{ass}^{1NN} is little larger than that of E_{ass}^{2NN}. This reveals that the oxygen vacancies prefer to be located at the 1NN site to Sm^{3+} ions. The associations between oxygen vacancies and Sm^{3+} ions are formed by the electrostatic attraction and the elastic interaction arising from the size mismatch of dopants compared to the host lattice [27]. Then the preferential distribution of oxygen vacancies can be the consequence of the delicate balance between electrostatic and elastic interactions in the crystalline lattice. Using DFT and KMC simulations, the results of vacancy-dopant association energies [13] and those of vacancy formation energies [28] at the 1NN and 2NN sites confirm the favorable distribution of oxygen vacancies around Sm^{3+} ions. The inhomogeneous distribution of oxygen vacancies causes the local distortion of the crystalline lattice.

Table 2. The vacancy-dopant association energies at 1NN and 2NN sites around Sm^{3+} ion.

Method	E_{ass}^{1NN} (eV)	E_{ass}^{2NN} (eV)
SMM	-0.1981	-0.128
DFT + MC [13]	-0.225	-0.135

Due to the reduced distance, the cation configuration at the 1NN sites around the saddle point B can impact strongly on the vacancy migration. There exist three possible types of cation configurations corresponding to three cation edges, namely, Ce^{4+}-Ce^{4+}, Ce^{4+}-Sm^{3+}, and Sm^{3+}-Sm^{3+} (Figure 3).

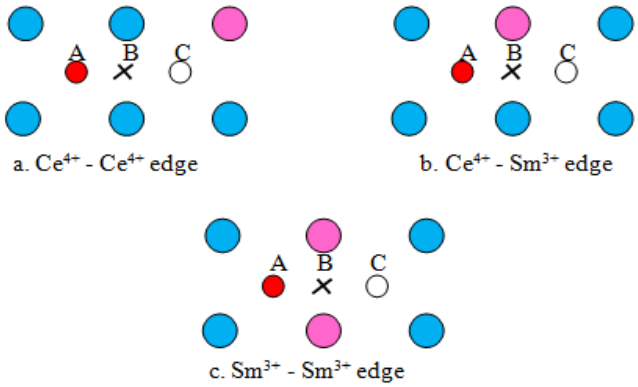

Figure 3. Possible migration edge configurations around the diffusing vacancy-oxygen ion pair in two-dimension plane. The blue and pink circles denote Ce^{4+} and Sm^{3+} ions, respectively.

The oxygen vacancies can jump into the adjacent sites containing oxygen ions by crossing these cation edges. The results of the migration energies across the cation edges are presented in Table 3.

One can see that the migration energy increases with the increasing dopant amount in the cation edge. The oxygen vacancy can migrate easily across the edge Ce^{4+}-Ce^{4+} without any dopant, while the number of available oxygen diffusion pathways is reduced by forming high energy Ce^{4+}-Sm^{3+} and Sm^{3+}-Sm^{3+} edges. The blocking effect is attributed to the narrow space for vacancy movement due to the large size of Sm^{3+} ions and the vacancy-dopant association. The influence of Sm^{3+} ion on the vacancy transport across the cation edge was also reported by the DFT and KMC methods [29, 30] at the different temperatures and dopant concentrations.

Table 3. The energies for vacancy migration across the cation edges.

Method	Ce^{4+}-Ce^{4+} (eV)	Ce^{4+}-Sm^{3+} (eV)	Sm^{3+}-Sm^{3+} (eV)
SMM	0.315	0.563	1.252
DFT + KMC [29]	0.527	0.696	1.1
DFT [30]	0.75	0.95	1.19

To understand the influence of vacancy-dopant association on the vacancy migration, we have calculated the Helmholtz free energies of crystalline lattice at the initial and final states with the different locations of Sm^{3+} ion at the 1NN sites around the migrating vacancy (Fig. 4) and then derive the migration energies. The cation configuration in Fig. 4a has a Sm^{3+} ion in the 1NN sites around the diffusing vacancy-oxygen ion pair. Our calculations show that the initial and final states have the same free energy. Indeed, the oxygen vacancy-oxygen ion exchange did not change the ionic configuration of the crystalline lattice. Hence, this configuration possesses the symmetric energy profile. However, more dopants reside in the 1NN sites around the diffusing vacancy (Figs. 4b and 4c) then the free energies at the final state are larger than those at the initial state.

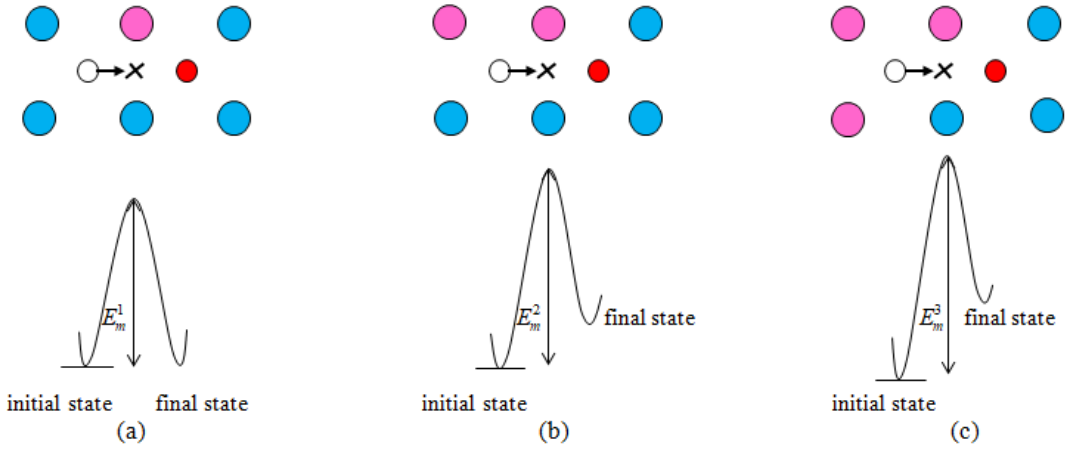

Figure 4. The trapping effect for the oxygen vacancy migration and the symmetric (a) and asymmetric (b), (c) energy profiles.

Consequently, the profiles in these situations become energetically asymmetric. The calculated migration energies with three configuration are E_m^1 = 0.563 eV, E_m^2 = 0.669 eV, and E_m^3 = 0.778 eV. The substitution of Ce^{4+} ions by Sm^{3+} ions at the 1NN sites around the oxygen vacancy generates the strong associations between the oxygen vacancy and Sm^{3+} ions at the shortest distance. These associations can deeply trap the oxygen vacancies and hinder the diffusion process.

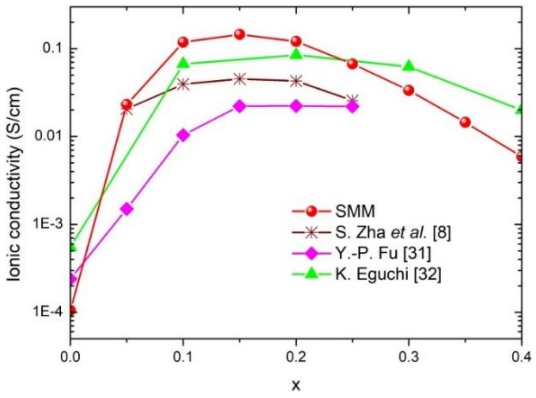

Figure 5. The dopant concentration dependence of ionic conductivity at T = 1073 K.

Figure 5 shows the curves of the ionic conductivity vs. the dopant concentration for a temperature of T = 1073 K. The ionic conductivity of SDC crystals exhibits an enhancement of roughly three orders of magnitude in comparison with that of CeO_2 crystal (x = 0). The ionic conductivity increases and then decreases with an increase in dopant concentration. The maximum value in ionic conductivity obtains at the dopant concentration x = 0.15. Initially, the number of oxygen vacancies is enhanced due to the increasing dopant concentration and consequently, the ionic conductivity increases quickly. However, after reaching a maximum value, it reduces due to the blocking and trapping effects on the vacancy migration. The high dopant concentration can lead to the creation of the high energy Ce^{4+}-Sm^{3+} and Sm^{3+}-Sm^{3+} edges and the strong associations between migrating vacancy and Sm^{3+} ions at the 1NN sites. The SMM results are consistent with experimental observations [8, 31, 32]. However, the calculated results are somewhat larger than most of the experimental results. This difference is attributed to neglecting the role of the oxygen vacancy-oxygen vacancy interaction in our study and the restriction on vacancy migration along grain boundaries in polycrystalline samples.

4. Conclusion

In this study, we have extended the SMM model to investigate the dopant effect on the structural and electrical properties of SDC crystals. The expressions of the average nearest-neighbor distance between two intermediate ions, the Helmholtz free energies of crystalline lattice at the different states are derived in closed analytic forms. The substitution of Ce^{4+} ions by Sm^{3+} ions leads to the lattice expansion and the local distortion of the crystalline lattice is the consequence of preferential distribution of oxygen vacancies at 1NN sites around dopants. Due to doping, the ionic conductivity of SDC crystals is in more than three orders of magnitude larger than that of undoped CeO_2 crystals. At high dopant concentration, the presence of Sm^{3+} ions in the cation edges and 1NN sites around the diffusing vacancy gives rise to the blocking and trapping effects on the vacancy migration. The ionic conductivity is a nonlinear function of the dopant concentration and reaches the maximum value at x = 0.15. Our calculation results are in agreement with the data published in both the theoretical and experimental works.

Acknowledgments

This research is financially supported by the Ministry of Education and Training of Vietnam under grant number B2021-TTB-02.

References

[1] P. Arunkumar, M. Meena, K. Suresh Babu, A Review on Cerium-Based Electrolytes for ITSOFC, Nanomaterials and Energy, Vol. 1, No. 5, 2015, pp. 288-305, https://doi.org/10.1680/nme.12.00015.

[2] A. Choudhury, H. Chandra, A. Arora, Application of Solid Oxide Fuel Cell Technology for Power Generation - A Review, Renewable and Sustainable Energy Reviews, Vol. 20, 2013, pp. 430-442, http://www.sciencedirect.com/science/article/pii/S1364032112006430.

[3] V. V. Sizov, M. J. Lampinen, A. Laaksonen, Molecular Dynamics Simulation of Oxygen Diffusion in Cubic Yttria-Stabilized Zirconia: Effects of Temperature and Composition, Solid State Ionics, Vol. 226, 2014, pp. 29-35, https://doi.org/10.1016/j.ssi.2014.08.003.

[4] M. Irshad, K. Siraj, R. Raza, A. Ali, A Brief Description of High Temperature Solid Oxide Fuel Cell's Operation, Materials, Design, Fabrication Technologies and Performance, Applied Sciences, Vol. 6, No. 3, 2016, pp. 75-98, https://doi.org/10.3390/app6030075.

[5] M. Coduri, S. Checchia, M. Longhi, D. Ceresoli, M. Scavini, Rare Earth Doped Ceria: The Complex Connection Between Structure and Properties, Frontiers in Chemistry, Vol. 6, 2018, pp. 526-1-526-23, https://www.frontiersin.org/articles/10.3389/fchem.2018.00526/full.

[6] S. Kuharuangrong, Ionic Conductivity of Sm, Gd, Dy and Er-Doped Ceria, Journal of Power Sources, Vol. 171, No. 2, 2007, pp. 506-510, https://doi.org/10.3389/fchem.2018.00526.

[7] H. Yahiro, Y. Eguchi, K. Eguchi, H. Arai, Oxygen Ion Conductivity of the Ceria-Samarium Oxide System with Fluorite Structure, Journal of Applied Electrochemistry, Vol. 18, 1988, pp. 527-531, https://link.springer.com/article/10.1007/BF01022246.

[8] S. Zha, C. Xia, G. Meng, Effect of Gd (Sm) Doping on Properties of Ceria Electrolyte for Solid Oxide Fuel Cells, Journal of Power Sources, Vol. 115, No. 1, 2003, pp. 44-48, https://doi.org/10.1016/S0378-7753(02)00625-0.

[9] S. Omar, E. D. Wachsman, J. L. Jones, J. C. Nino, Crystal Structure-Ionic Conductivity Relationships in Doped Ceria Systems, J. Am. Ceram. Soc., Vol. 92, No. 11, 2009, pp. 2674-2681, https://doi.org/10.1111/j.1551-2916.2009.03273.x.

[10] T. Shimonosono, Y. Hirata, Y. Ehira, S. Sameshima, T. Horita, H. Yokokawa, Electronic Conductivity Measurement of Sm- and La-Doped Ceria Ceramics by Hebb–Wagner Method, Solid State Ionics, Vol. 174, No. 1-4, 2004, pp. 27-33, https://doi.org/10.1016/j.ssi.2004.07.025.

[11] J. Koettgen and M. Martin, The Ionic Conductivity of Sm-Doped Ceria, J. Am. Ceram. Soc., Vol. 103. No. 6, 2020, pp. 3776-3787, https://doi.org/10.1111/jace.17066.

[12] Z. Zhan, T. -L. Wen, H. Tu, Z. -Y. Lu, AC Impedance Investigation of Samarium-Doped Ceria, Journal of The Electrochemical Society, Vol. 148, 2001, pp. A427-A432, https://doi.org/10.1149/1.1359198.

[13] S. Grieshammer, B. O. H. Grope, J. Koettgen, M. Martin, A Combined DFT + U and Monte Carlo Study on Rare Earth Doped Ceria, Phys. Chem. Chem. Phys., Vol. 16, 2014, pp. 9974-9986, https://doi.org/10.1039/C3CP54811B.

[14] Z. Fu, Q. Sun, D. Ma, N. Zhang, Y. An, Z. Yang, Effects of Sm Doping Content on the Ionic Conduction of CeO_2 in SOFCs from First Principles, Appl. Phys. Lett., Vol. 111, No. 2, 2017, pp. 023903-1-023903-5, https://doi.org/10.1063/1.4993897.

[15] A. Ismail, J. Hooper, J. B. Giorgi, T. K. Woo, A DFT+U Study of Defect Association and Oxygen Migration in Samarium-Doped Ceria, Phys. Chem. Chem. Phys, Vol. 13, 2011, pp. 6116-6124, https://doi.org/10.1039/C0CP02062A.

[16] S. Omar, E. D. Wachsman, J. L. Jones, J. C. Nino, Crystal Structure-Ionic Conductivity Relationships in Doped Ceria Systems, J. Am. Ceram. Soc., Vol. 92, No. 11, 2009, pp. 2674-2681, https://doi.org/10.1111/j.1551-2916.2009.03273.x.

[17] L. T. Lam, V. V. Hung, N. T. Hai, Study of Oxygen Vacancy Diffusion in Yttria doped Ceria and Yttria-Stabilized Zirconia by Statistical Moment Method, Communications in Physics. Vol. 29, No. 3, 2019, pp. 263-276.

[18] L. T. Lam, V. V. Hung, B. D. Tinh, Investigation of the Ionic Conductivities of Yttria-Doped Ceria and Yttria-Stabilized Zirconia by Using the Statistical Moment Method, Journal of the Korean Physical Society, Vol. 75, 2019, pp. 293-303, https://doi.org/10.3938/jkps.75.293.